



# Interpretation of Adjoint Solutions for Turbomachinery Flows

Andre C. Marta\*

*Instituto Superior Técnico, Lisbon 1049, Portugal*

Sriram Shankaran†

*General Electric, Niskayuna, New York 12309*

Qiqi Wang‡

*Massachusetts Institute of Technology, Cambridge, Massachusetts 02139*

and

Prem Venugopal§

*General Electric, Niskayuna, New York 12309*

DOI: 10.2514/1.J052177

Although the mathematical derivation of the adjoint equations and their numerical implementation is well established, there is scant discussion on the understanding of the adjoint solution by itself. As this is a field solution of similar resolution of the flowfield, there is a wealth of data that can be used for design guidance. The aim is to tie the adjoint solution to the flowfield, which has physical properties. The adjoint solution of four representative cases taken from turbomachinery aerodynamic problems are used to identify the physical insight it provides. The focus is on changes related to geometry, but the changes can also be realized using other inputs to the flow solver (e.g., boundary conditions). It is shown how the adjoint counterpart of the density and velocity field can be used to provide insights into the nature of changes the designer can induce to cause improvement in the performance metric of interest. Discussion on how to use adjoint solutions for problems with constraints to further refine the changes is also included. Finally, a turbine strut problem is discussed where it is not immediately apparent what geometry changes need to be used for further evaluation with optimization algorithms. The adjoint and flow solutions are used to determine the kind of end-wall treatments that reduce the loss. These changes are then implemented to show that the loss is actually reduced. The results in this paper show there is a twofold use of the adjoint method: one for guiding the automatic optimization as such and the second for guiding the designer in the choice of the design space.

## Nomenclature

|               |  |
|---------------|--|
| $B$           | = body force term for each cell        |
| $C$           | = constraint functions                 |
| $c$           | = convective speed                     |
| $E$           | = energy                               |
| $\mathcal{F}$ | = objective function                   |
| $g$           | = gradient vector                      |
| $k$           | = turbulence kinetic energy            |
| $l$           | = length of domain                     |
| $\hat{n}_i$   | = normal vector at cell face $i$       |
| $p$           | = pressure                             |
| $\mathcal{R}$ | = residual operator                    |
| RHO           | = adjoint density                      |
| $S$           | = vector of dependent design variables |
| $T$           | = terminal time                        |
| $t$           | = time                                 |
| $u$           | = convected quantity                   |
| $u_i$         | = velocity components                  |
| $w$           | = state vector for flow equations      |
| $x_j$         | = coordinate direction                 |

|             |                               |
|-------------|-------------------------------|
| $\alpha$    | = independent design variable |
| $\rho$      | = density                     |
| $\tau_{ji}$ | = stress tensor               |
| $\psi$      | = adjoint field               |
| $\omega$    | = specific dissipation rate   |

## I. Introduction

THE continuous growth of computational power has made external and internal flow simulations to be routinely performed using high-fidelity computational fluid dynamic (CFD) models. The emerging trend is to use optimization techniques as part of the design tools, with numerical design optimization becoming common practice not only in academia but also in industry.

Among the several optimization methods developed by the operations research field [1], and considering that CFD flow simulations can take hours, if not days, to perform, the most efficient methods are gradient-based, which require a minimal number of cost-function evaluations. However, these methods require an estimate of the cost-function derivatives. To address this, the designer faces the problem of evaluating the derivatives [2]. Finite-difference approximations have always been popular due to their simplicity, but they rapidly become computationally prohibitive when the number of variables greatly exceeds the number of functions. Although the cost of finite differences is proportional to the number of design variables, the cost of the adjoint method is proportional to the number of objective functions. Thus, in case the number of design variables greatly exceeds the number of objective functions, the adjoint method is the best-suited approach to efficiently estimate function gradients because the cost involved in calculating sensitivities using the adjoint method is practically independent of the number of design variables.

Received 19 July 2012; revision received 28 January 2013; accepted for publication 30 January 2013; published online 20 May 2013. Copyright © 2013 by the authors. Published by the American Institute of Aeronautics and Astronautics, Inc., with permission. Copies of this paper may be made for personal or internal use, on condition that the copier pay the \$10.00 per-copy fee to the Copyright Clearance Center, Inc., 222 Rosewood Drive, Danvers, MA 01923; include the code 1533-385X/13 and \$10.00 in correspondence with the CCC.

\*Researcher, Center for Aerospace Science and Technology, Avenida Rovisco Pais 1. Member AIAA.

†Mechanical Engineer, Fluid Mechanics Lab., Global Research Center, 1 Research Circle. Member AIAA.

‡Assistant Professor, Department of Aeronautics, 77 Massachusetts Avenue. Member AIAA.

§Mechanical Engineer, Turbomachinery Aerodynamics Lab., Global Research Center, 1 Research Circle. Member AIAA.

The application of adjoint methods to CFD was pioneered by Pironneau [3], and it was later revisited and extended by Jameson [4] and Jameson et al. [5] to perform airfoil and wing design, respectively. More recent successful applications include multipoint aerodynamic shape optimization problems [6], aerostructural design optimization [7], and even magnetohydrodynamics flow control [8].

There are roughly two approaches to developing adjoints: a continuous one and a discrete approach. The reader is referred to [9,10] for an introduction to adjoints and detailed discussions of the two approaches and their benefits and drawbacks.

It should be noted, though, that gradient-based methods can be of limited use because of their local nature, being just one of the options, with global optimization being often the preferred choice. However, the adjoint-based sensitivities can be used either directly in gradient-based optimization that leads to local optimum or in conjunction with surrogate models like kriging to obtain global optima. Recent studies have successfully used the adjoint method in conjunction with surrogate models for global optimization techniques [11–13].

The major drawback of using adjoint-based gradients has always been the necessity of implementing an additional solver: the adjoint system of equations solver, which is generally of the same complexity as the flow solver. Thus, in the presence of flows modeled by the Reynolds-averaged Navier–Stokes (RANS) equations, the corresponding adjoint system might become far too complex to be fully derived. This has led to the use of many approximations and simplifications in the implementation of such adjoint solvers. Among the different approaches found in the literature, the major ones are:

*Euler equations:* Both the flow and adjoint solvers only account for the inviscid flow effects. The argument is that, in some external flows, such as in clean aircraft configurations, and in some internal flows, such as in some turbine blades, the viscous effects can be neglected because there are no regions of flow separation [14].

*RANS with algebraic turbulence models:* The adjoint solver is consistent with the flow solver, but a simplistic turbulence model is used to expedite the development of the former solver. Often used when the viscous and turbulent effects need to be accounted for, but the development effort is kept to a minimum [15].

*RANS with constant-eddy viscosity (CEV) approximation:* The flow solver uses proper two-equation turbulence models, such as  $\kappa$ - $\epsilon$  or  $\kappa$ - $\omega$ , but the adjoint solver assumes frozen eddy viscosity. In this case, the flow is properly solved, and it is assumed that the variation of viscosity can be neglected in the adjoint [16,17].

*RANS flow and adjoint solver:* This corresponds to the exact derivation of the adjoint solver, regardless of the complexity of the turbulence model used. The dual (adjoint) solver is perfectly consistent with the primal (flow) solver. This approach is made feasible if one uses the hybrid ADjoint methodology to develop the adjoint solver [18,19], where automatic differentiation (AD) is used to assist its implementation.

These approaches are all used today by the adjoint-based design community, but there is no clear evidence of what are the penalties associated with approximation models compared to the exact adjoint solver, when using the adjoint solution to drive a realistic gradient-based optimization problem.

Traditionally the process of selecting design variations has been carried out by trial and error, relying on the intuition and experience of the designer. It is not at all likely that repeated trials using an interactive design and analysis procedure can lead to a truly optimum design. Even more systematic approaches such as design of experiments (DOE) lose to adjoint methods because the cost of the former scale with the number of variables. To take full advantage of the possibility of examining a large design space, the numerical simulations need to be combined with automatic search and optimization procedures. However, the realizable improvements are limited by the capability of the CFD model to capture the flow physics.

## II. Background

The underlying theory of adjoint-based high-fidelity CFD design optimization is presented next. Typical use of the adjoint in a design environment involves the following steps: 1) obtain a steady flow-field, and 2) obtain a adjoint field.

### A. Generic Design Problem

A generic CFD design problem can be formally described as

$$\begin{aligned} & \text{Minimize } \mathcal{F}(w, S(\alpha)) \\ & \text{w.r.t. } \alpha \\ & \text{subject to } \mathcal{R}(w, S(\alpha)) = 0 \\ & C(w, S(\alpha)) = 0 \end{aligned} \quad (1)$$

where  $\mathcal{F}$  is the cost-function vector,  $S$  and  $\alpha$  are the dependent and independent (respectively) set of design variables,  $w$  is the flow solution (which is typically of function of the design variables), and  $C = 0$  represents additional constraints that may or may not involve the flow solution. The distinction is made between  $S$  and  $\alpha$  to reflect the geometry kernels of common design environments, where quantities that the designer alters are engineering parameters, like stagger or thickness, are lumped in  $\alpha$ , while  $S$  represents the CFD mesh points.

The flow-governing equations expressed in the form  $\mathcal{R} = 0$  also appear as a constraint because the solution  $w$  must always obey the flow physics.

When using a gradient-based optimizer to solve the design problem [Eq. (1)], the evaluation of the cost and constraint functions as well as their gradients with respect to the design variables are required, that is  $\frac{\partial \mathcal{F}}{\partial \alpha}$  and  $\frac{\partial \mathcal{C}_i}{\partial \alpha}$  have to be estimated.

### B. Flow-Governing Equations

The governing equations used in the present work are the RANS equations. In conservation form, the Navier–Stokes system of equations may be written in index notation as

$$\frac{\partial \rho}{\partial t} + \frac{\partial}{\partial x_j} (\rho u_j) = 0 \quad (2a)$$

$$\frac{\partial}{\partial t} (\rho u_i) + \frac{\partial}{\partial x_j} (\rho u_i u_j + p \delta_{ij} - \tau_{ji}) = 0, \quad i = 1, 2, 3 \quad (2b)$$

$$\frac{\partial}{\partial t} (\rho E) + \frac{\partial}{\partial x_j} (\rho E u_j + p u_j - u_i \tau_{ij} + q_j) = 0 \quad (2c)$$

where  $\rho$ ,  $u_i$ , and  $E$  are the density, mean velocity, and total energy, respectively;  $p$  is the pressure;  $\tau_{ij}$  is the viscous stress; and  $q_j$  is the heat flux.

A turbulence model needs to be used to model the Reynolds stresses. In this paper, a two-equation turbulence model was used, in particular the  $k$ - $\omega$  model of [20]:

$$\begin{aligned} \frac{\partial}{\partial t} (\rho k) + \frac{\partial}{\partial x_j} (\rho k u_j) &= \tau_{ij} \frac{\partial u_i}{\partial x_j} - \beta_k \rho k \omega \\ &+ \frac{\partial}{\partial x_j} \left[ \left( \mu + \sigma_k \frac{\rho k}{\omega} \right) \frac{\partial k}{\partial x_j} \right] \end{aligned} \quad (3a)$$

$$\begin{aligned} \frac{\partial}{\partial t} (\rho \omega) + \frac{\partial}{\partial x_j} (\rho \omega u_j) &= \frac{\gamma \omega}{k} \tau_{ij} \frac{\partial u_i}{\partial x_j} - \beta_\omega \rho \omega^2 \\ &+ \frac{\partial}{\partial x_j} \left[ \left( \mu + \sigma_\omega \frac{\rho k}{\omega} \right) \frac{\partial \omega}{\partial x_j} \right] \end{aligned} \quad (3b)$$

where  $k$  is the turbulence kinetic energy, and  $\omega$  is the specific dissipation rate. The turbulent eddy viscosity is computed from  $\mu_T = \rho k / \omega$ , and the constants are  $\gamma = 5/9$ ,  $\beta_k = 9/100$ ,  $\beta_\omega = 3/40$ ,  $\sigma_k = 1/2$ , and  $\sigma_\omega = 1/2$ . The effective viscosity used in the Navier–Stokes equation [Eq. (2)] is then computed as  $\mu = \mu_m + \mu_T$ , where  $\mu_m$  is the molecular (laminar) viscosity.

In semidiscrete form, the RANS governing equations [Eqs. (2) and (3)] can be expressed as

$$\frac{dw_{ijk}}{dt} + \mathcal{R}_{ijk}(w) = 0 \quad (4)$$

where  $w = (\rho, \rho\mathbf{u}, \rho E, \rho k, \rho w)^T$  is the vector of conservative variables,  $\mathcal{R}$  is the residual with all of its components (inviscid, viscous, and turbulent fluxes, boundary conditions, and artificial dissipation), and the triad  $ijk$  represents the three computational directions. The unsteady term of Eq. (4) is dropped out because only the steady solution of the equation is of interest in this work.

### C. Adjoint Equations

The adjoint equations can be derived using the approach in [10] or [9]. A brief overview of the adjoint process for deterministic systems is first provided and then described in the context of Euler (or Navier–Stokes) equations that govern the evolution of fluid flow. The cost-function vector is a function of the state variables  $w$  and the control variables  $S$ , which may be represented by the function  $\mathcal{F}$ . Then,

$$\mathcal{F} = \mathcal{F}(w, S(\alpha)) \quad (5)$$

and a change in  $S$  results in a change

$$\delta\mathcal{F} = \frac{\partial\mathcal{F}}{\partial w}\delta w + \frac{\partial\mathcal{F}}{\partial S}\delta S \quad (6)$$

in the cost function. Using control theory, the governing equations for the state variables are introduced as a constraint in such a way that the final expression for the gradient does not require re-evaluation of the state. To achieve this,  $\delta w$  must be eliminated from Eq. (6). Suppose that the governing equation  $\mathcal{R}$ , which expresses the dependence of  $w$  and  $S$  within the domain  $D$ , can be written as

$$\mathcal{R}(w, S) = 0 \quad (7)$$

Then,  $\delta w$  is determined from the equation

$$\delta\mathcal{R} = \left[ \frac{\partial\mathcal{R}}{\partial w} \right] \delta w + \left[ \frac{\partial\mathcal{R}}{\partial S} \right] \delta S = 0 \quad (8)$$

Next, introducing a Lagrange multiplier  $\psi$  yields

$$\begin{aligned} \delta\mathcal{F} &= \frac{\partial\mathcal{F}}{\partial w}\delta w + \frac{\partial\mathcal{F}}{\partial S}\delta S - \psi^T \left( \left[ \frac{\partial\mathcal{R}}{\partial w} \right] \delta w + \left[ \frac{\partial\mathcal{R}}{\partial S} \right] \delta S \right) \\ &= \left( \frac{\partial\mathcal{F}}{\partial w} - \psi^T \left[ \frac{\partial\mathcal{R}}{\partial w} \right] \right) \delta w + \left( \frac{\partial\mathcal{F}}{\partial S} - \psi^T \left[ \frac{\partial\mathcal{R}}{\partial S} \right] \right) \delta S \end{aligned} \quad (9)$$

To eliminate  $\delta w$  implies

$$\left[ \frac{\partial\mathcal{R}}{\partial w} \right]^T \psi = \frac{\partial\mathcal{F}}{\partial w} \quad (10)$$

resulting in

$$\delta\mathcal{F} = \mathcal{G}\delta S \quad (11)$$

where

$$\mathcal{G} = \frac{\partial\mathcal{F}}{\partial S} - \psi^T \left[ \frac{\partial\mathcal{R}}{\partial S} \right] \quad (12)$$

This process allows for elimination of the terms that depend on the flow solution with the result that the gradient with respect to an arbitrary number of design variables can be determined without the need for additional evaluations of the state. Now, the adjoint equations can be written as

$$\left[ \frac{\partial\mathcal{R}}{\partial w} \right]^T \psi = \left[ \frac{\partial\mathcal{F}}{\partial w} \right] \quad (13)$$

where  $\psi$  is the adjoint vector.

Because the CFD solver does not handle the geometric parameters  $\alpha$  directly, but rather a computational mesh defined by the coordinates of each node  $S$ , the chain rule of differentiation is used to express the gradient of the cost function with respect to the design variables as

$$\frac{d\mathcal{F}}{d\alpha} = \frac{d\mathcal{F}}{dS} \frac{dS}{d\alpha} \quad (14)$$

being the total gradient of the cost function with respect to the grid coordinates, based on the adjoint solution  $\psi$ , given by

$$\frac{d\mathcal{F}}{dS} = \frac{\partial\mathcal{F}}{\partial S} - \psi^T \frac{\partial\mathcal{R}}{\partial S} \quad (15)$$

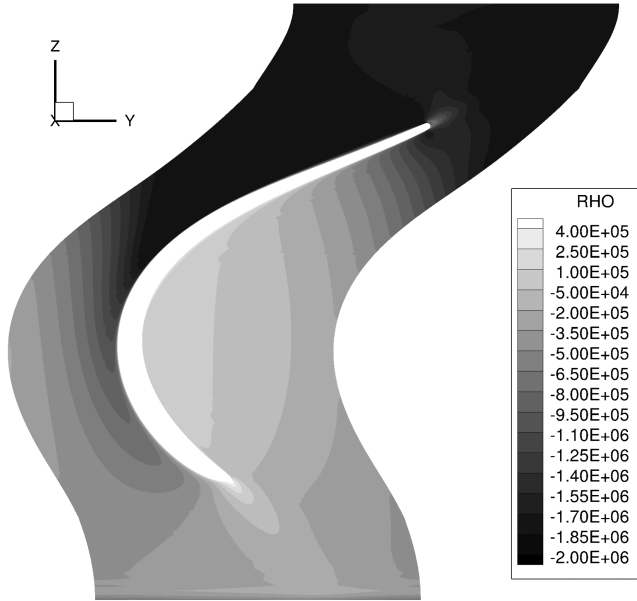
The evaluation of the gradient of each cost or constraint function in the optimization problem Eq. (1) requires solving Eq. (13) with a new right-hand-side vector. If the optimization problem has constraints  $C$ , then an additional adjoint equation is solved for each  $C$  (instead of  $\mathcal{F}$ ) and the gradient of the objective  $\mathcal{F}$  and  $C$  used in the optimizer. The optimizer enforces the constraint using the value  $C$  and its constraints. On the other hand, the computational cost of the total sensitivity Eq. (15) is almost independent of the number of grid coordinates, which is the feature that makes the adjoint method so attractive for gradient-based optimization involving a large number of design variables and a few functions.

### D. Interpreting the Adjoint Solutions

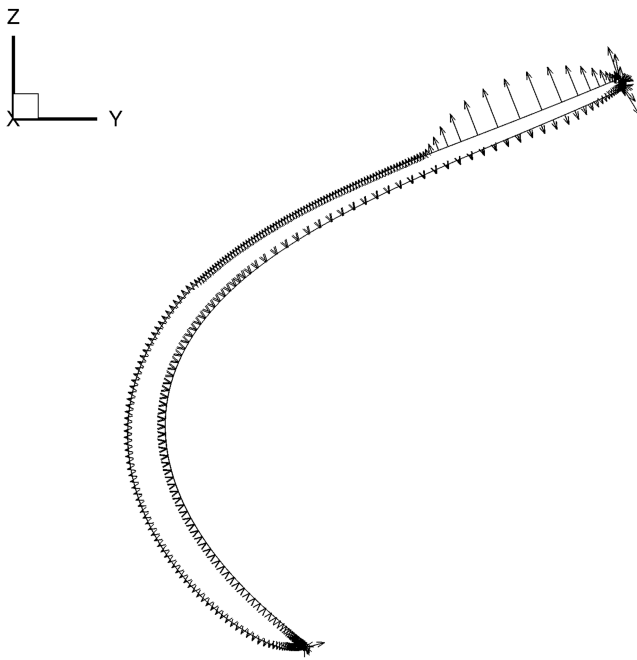
The key to reading the adjoint solution is the observation that the product of the adjoint vector,  $\psi$ , and the variation in the constraint,  $\delta\mathcal{R}$ , determines the change to the objective function. This is just a rewording of the statement that the adjoint vector is the Lagrange multiplier. However, on closer inspection, this statement can be strengthened in the context of the constraint equations being the Navier–Stokes equations. A brief highlight is given in this paragraph, and the subsequent material in this subsection derives the equations that back the assertions. In this case, the adjoint solution at each grid point, which is a vector counterpart to the flow solution at that grid point, has a one-to-one correspondence to the flow solution. For example, the adjoint counterpart for density can be interpreted as the change required to be induced to the mass flux to cause an increase in the objective function of interest. Similarly, the adjoint counterpart for the turbulence quantities signifies the change required in the turbulent flux to increase the objective function. It is common for many problems to observe that the adjoint solution has positive or negative signs at different points in the computational domain. In such cases, the interpretation can be made stronger. Here, the design guidance that the adjoint solution provides is to require that the designer induce changes that increase density flux where the adjoint solution is positive and decrease density flux where the adjoint solution is negative.

The reader is referred to the Appendix for a discussion on the one-dimensional time-dependent linear equation, but the focus is now on the flow equations represented by Euler and Navier–Stokes equations. These equations being nonlinear and in coupled form make it trickier to analyze. To ground the discussion, a turbine vane is taken as example. Figure 1 shows the contours of the adjoint variable corresponding to density for a turbine vane (the flow is from the bottom of the page to the top) and the gradient vector plot on the surface of the airfoil for the loss coefficient. The vector points in the direction of surface movement that leads to increase in loss. The range of the adjoint solution spans the positive and negative real axis, suggesting that improvements in the metric (in this case, loss, which ought to be reduced) can be obtained by decreasing the density over the suction side of the airfoil while mostly increasing it over the fore portion of the pressure side. In relative magnitude, the suggested reduction in density near the trailing edge of the suction side is more than over the same region on the pressure side.

The loss metric is defined as the drop in total pressure across the domain, appropriately normalized. The boundary condition applied at the inlet holds the total pressure to the prescribed value and under the assumption that the static pressure variations at the inlet are small (weak upstream traveling waves), the major contribution to the



a) Adjoint density contours



b) Gradient vector plot

Fig. 1 Two-dimensional vane adjoint and gradients ( $d\eta/dx$ ).

change in loss is the change to the exit total pressure. Any increase in the exit total pressure leads to a reduction in the loss metric.

If geometry changes that alter the density flux are made as suggested by the adjoint solution, the fore portion of the suction side will decelerate the flow by reducing the curvature and the mid-to-aft portion will accelerate the flow by changing the turning angle of the metal. The former will increase the density, and the latter will decrease the density. On the pressure side, the suggested geometry changes push the axial location of the maximum pressure aft, while simultaneously providing a steeper pressure gradient in the aft portion. From a loss budget perspective, the suggested changes increase the diffusion factor (ratio of peak Mach number to trailing edge Mach number), and hence the reduction in loss has to be due to the possible decrease in viscous profile losses.

Before a mathematical foundation is provided to interpret the adjoint solution, a sketch of the thought process is presented using the one-dimensional Euler equations. The sensitivity of the cost

functional with respect to changes in the geometry can be written following Eq. (15) as

$$\frac{d\mathcal{F}}{dx} = \left( \frac{\partial \mathcal{F}}{\partial x} - \psi^T \frac{\partial \bar{\mathcal{R}}}{\partial x} \right) - \psi^T \frac{\partial \bar{\mathcal{R}}}{\partial x} \quad (16)$$

where  $\bar{\mathcal{R}}$  is the nominal residual, and  $\tilde{\mathcal{R}}$  is the contribution to the residual due to reduction in density flux. Typically, one computes  $\mathcal{R} = \mathcal{R}_i - \mathcal{D}_i$ , where the first term in the inviscid contribution, and the second is the dissipation contribution.

One can write the discrete form of the numerical scheme and try to perform the analysis. However, following this path of analysis necessitates the need to consider changes to residual of the neighboring cells requiring more assumptions to justify the premise of this section. Instead, if one considers the possibility of adding a mass-flux source (or equivalently a body force) term to increase the residual, then one can proceed on a cell-by-cell basis. Consider the following possibility: if one manages to introduce a mass-flux source (or body force) term in a cell where the adjoint is positive, then the residual in that cell will now increase. Because this is done for each cell, it does not involve interactions from other neighboring cells in the discretization stencil. Thus, in essence, when the adjoint is positive in a cell, if one can induce a geometry change that increases the mass flux in that cell (through a body force for mass), then the residual increases and hence one can cause an overall increase in the variation of  $\mathcal{F}$ . After this brief overview, a stronger theoretical basis is now provided.

The relationship between the body force (source terms) and the geometric change is through the residual  $\mathcal{R}$ . Let  $\mathcal{R}(w, x) = 0$  be the operator form of the governing equations. When the geometry changes by  $dx$ , then the residual  $\mathcal{R}(w, x + dx) = \frac{d\mathcal{R}}{dx} dx$ . Denote this as *resid*. If the governing equations are solved on a perturbed mesh, the change in flow,  $dw$ , must satisfy  $\mathcal{R}(w + dw, x + dx) = \mathcal{R}(w, x) + \frac{d\mathcal{R}}{dx} dx + \frac{d\mathcal{R}}{dw} dw = 0$  or  $\frac{d\mathcal{R}}{dw} dw = -\text{resid}$ . This is special because it will be seen that *resid* will be the appropriate body force to use.

Suppose a “forced” governing equation is solved, on the unperturbed mesh, driven by  $-\text{resid}$ , for  $w^1$  such that  $\mathcal{R}(w^1, x) = -\text{resid}$ . Then  $w^1 = w + dw$ . This means that the following two equations have the same solution  $w^1$ :

$$\mathcal{R}(w + dw, x) = -\text{resid} \quad (17)$$

$$\mathcal{R}(w + dw, x + dx) = 0 \quad (18)$$

In other words, one can “simulate” the flow-field with the perturbed geometry by using the original geometry but adding a forcing term equal to  $-\text{resid}$ . Therefore, to calculate the “equivalent” forcing term that can simulate a perturbed geometry, one needs to calculate the residual of the original flowfield on the perturbed geometry.

To make the connection to our primary premise that the adjoint field can provide information on how to change the geometry, consider writing the governing equations in the following form with a body force:

$$\mathcal{R}(w, x) + B(x) = 0 \quad (19)$$

Assume that, for the unperturbed geometry,  $B(x) = 0$ . As  $B$  depends on the geometry, after solving for the adjoint field, the gradient expression can be written as

$$\frac{d\mathcal{F}}{dx} = \left( \frac{\partial \mathcal{F}}{\partial x} - \psi^T \frac{\partial \bar{\mathcal{R}}}{\partial x} \right) - \psi^T \frac{\partial B}{\partial x} \quad (20)$$

Now, when the adjoint solution is positive, say, if a geometry change is introduced such that  $B$  for the cell is increased then it will decrease the cost function. Thus, if one introduces a body force in the domain of the same sign as the adjoint, one can increase the cost function. Please note that, as one is making changes to  $x$  to induce a particular

change to  $\tilde{\mathcal{R}}$ , one is in effect directly altering  $\frac{\partial \tilde{\mathcal{R}}}{\partial \mathbf{x}}$ . Similar arguments can also be made with the adjoint field for the momentum, energy, and turbulence quantities. For example, for the momentum equations, a change in geometry that induces a body-force-like term for that cell results in an increase (or decrease) in residual for that cell.

This approach of interpreting the adjoint solutions is particularly useful when it is known a priori what geometry changes will help to improve the overall metric. Although a similar conclusion can be drawn from investigating the gradient vector plot, interpreting the adjoint solution provides the designer a mechanism to relate the geometry changes to changes in the flowfield. Hence, it provides a form of design guidance for the designer while also allowing the designer to be cognizant of changes to other metrics that are either posed as constraints to the optimization problem or not posed at all.

### III. Implementation

The development of the flow and adjoint solvers and the adjoint treatment of the turbulence equations are described next.

#### A. Flow Solver

The flow solver for a steady-state solution is an explicit solver with four- or five-stage Runge–Kutta scheme, using multigrid and residual averaging for convergence acceleration. The spatial discretization is second-order with a Jameson–Schmidt–Turkel (JST) scheme [21] for artificial dissipation. The flow solver used in this work supports three-dimensional, multi-block, structured grids, and it uses a finite-volume formulation of the nonlinear and linear RANS equations. Several turbulence models are available, such as  $k-\omega$  [20,22],  $k-\epsilon$  [23], and SST [24], having the option to use wall functions or wall integration for boundary-layer resolution. This solver is typically employed in the solution of turbomachinery blade rows, and it is capable of efficiently performing three-dimensional analysis for aeromechanics, aerodynamic design, parametric studies, and robust design applications.

#### B. Adjoint Solver

The simple mathematical form of Eq. (13) can be very misleading because, depending on the approach, its numerical implementation can be quite complex, if derived by manual differentiation, or relatively costly, if derived using finite-differences. The latter also brings issues in the accuracy of the derivatives and the choice of step sizes.

When it comes to implementation, there are two main ways of obtaining the adjoint equations Eq. (13) for a given system of PDEs. These two adjoint formulations can be classified into continuous or discrete. The continuous adjoint approach forms a continuous adjoint problem from the governing PDEs and then discretizes this problem to solve it numerically. The discrete adjoint approach first discretizes the governing PDE and then derives an adjoint system for these discrete equations. As such, there is freedom as how to discretize the adjoint PDE using the continuous approach, whereas the adjoint implementation in the discrete approach is fixed by the primal discretization.

A discrete adjoint approach formulation is chosen because it can be applied to any set of governing equations, and it can treat arbitrary cost functions. As such, and in contrast to the continuous approach, no simplifications have to be made during the derivation; the effects of viscosity and heat transfer and the turbulence equations can be easily handled when deriving the discrete adjoint.

But the most interesting feature of the discrete approach is that it allows the use of AD tools [25] in its derivation, expediting considerably the process of obtaining the differentiated form of the discretized governing equations necessary to assemble the adjoint system of equations.

As such, the approach used in this work is hybrid, and it follows the work of [18,19]. The discrete adjoint solver is derived with the aid of an automatic differentiation tool that is selectively applied to the CFD source code that handles the residual and function evaluations. This tool produces the routines that evaluate the partial derivative matrices

$\partial \mathcal{R} / \partial \mathbf{w}$ ,  $\partial \mathcal{F} / \partial \mathbf{w}$ ,  $\partial \mathcal{F} / \partial \mathbf{x}$ , and  $\partial \mathcal{R} / \partial \mathbf{x}$  that are necessary to compute gradients [Eq. (15)] using the adjoint method [Eq. (13)]. This hybrid approach retains the accuracy of the adjoint methods, while it adds the ease of implementation of the automatic differentiation methods. The AD tool chosen in this work is Tapenade [26] because it supports Fortran 90, which is a requirement taking into account the programming language used in the flow solver.

The sizes of the matrices involved in this process are

$$\begin{aligned} \frac{\partial \mathcal{R}}{\partial \mathbf{w}} &(N_w \times N_w), & \frac{\partial \mathcal{F}}{\partial \mathbf{w}} &(N_{\mathcal{F}} \times N_w), \\ \frac{\partial \mathcal{R}}{\partial \mathbf{x}} &(N_w \times N_x), & \frac{\partial \mathcal{F}}{\partial \mathbf{x}} &(N_{\mathcal{F}} \times N_x) \end{aligned} \quad (21)$$

where  $N_{\mathcal{F}}$  is the number of cost functions,  $N_x$  is the number of grid coordinates and  $N_w$  is the size of the state vector. The size of the vector  $\mathbf{w}$  depends on the number of governing equations,  $N_e$ , and the number of cells of the computational mesh,  $N_c$ , that discretize the physical domain, according to the relation  $N_w = N_e \times N_c$ , which for the solution of a large, three-dimensional problem involving a system of conservation laws, can be very large. The size of the grid coordinates vector  $\mathbf{x}$  is given by dimensionality of the problem times the number of vertices corresponding to the computational mesh used, that is  $N_x = 3 \times N_v$  for three-dimensional problems.

Because a discrete approach is used, the boundary conditions for the adjoint equations are not explicitly enforced. However, the current implementation corresponds to the imposition of the adjoint counterpart of pressure for the one upstream boundary, and the other four downstream conditions correspond to the conservative variables  $\rho$ ,  $\rho u$ ,  $\rho v$ , and  $\rho w$ .

The adjoint linear system [Eq. (13)] has to be solved  $N_{\mathcal{F}}$  times because  $\psi$  is valid for all grid coordinates  $\mathbf{x}$  but must be recomputed for each function  $\mathcal{F}$ . To solve this large sparse discrete adjoint problem, the Portable, Extensible Toolkit for Scientific Computation (PETSc) [27] is used. The adjoint system of equations is solved using a PETSc built-in Krylov subspace method, more specifically, the generalized minimum residual method [28] with the incomplete factorization preconditioner with one level fill, ILU(1) preconditioner.

Once the adjoint solution  $\psi$  is found, the gradient of the cost function with respect to the grid coordinates is obtained from Eq. (15), which implies a simple matrix-vector multiplication operation.

#### C. Constant-Eddy Viscosity Approximation

The full RANS adjoint solver described so far makes use of the complete vector of conservative variables and handles the corresponding seven governing equations [Eqs. (2) and (3)].

The CEV approximation still solves the full RANS flow equations, but it assumes that the variation of the turbulent eddy viscosity  $\mu_T$  can be neglected in the derivation of the adjoint equations. Therefore, under the CEV assumption, only five equations [Eq. (2)] are used to derive the adjoint, which significantly reduces the size of the dual problem, as quantified in Eq. (21). The benefits are an easier implementation, faster run time, and reduced memory requirements. The authors' primary interest in using this approximation is to reduce the computational cost of the adjoint analysis, an important criterion due to the memory requirements of the matrix solver. However, it has also been noticed that, for problems where the steady flow solver fails to converge to within numerical round-off, the convergence of the adjoint can be improved using the constant eddy viscosity approach. The reader is referred to [29,30] for a detailed description of the use of constant eddy viscosity approaches for adjoint equations.

The matrix  $\partial \mathcal{R} / \partial \mathbf{w}$  is reduced by a factor of  $7^2 / 5^2 = 1.96$ , and the vector  $\partial \mathcal{F} / \partial \mathbf{w}$  and matrix  $\partial \mathcal{R} / \partial \mathbf{x}$  are reduced by a factor of  $7/5 = 1.4$ .

In the present adjoint solver implementation, a single flag controls whether CEV approximation is to be used. If so, the adjoint system does not include the counterpart to the flow turbulent equations, and the turbulent eddy viscosity is retrieved from the flow solution and used in the adjoint system.

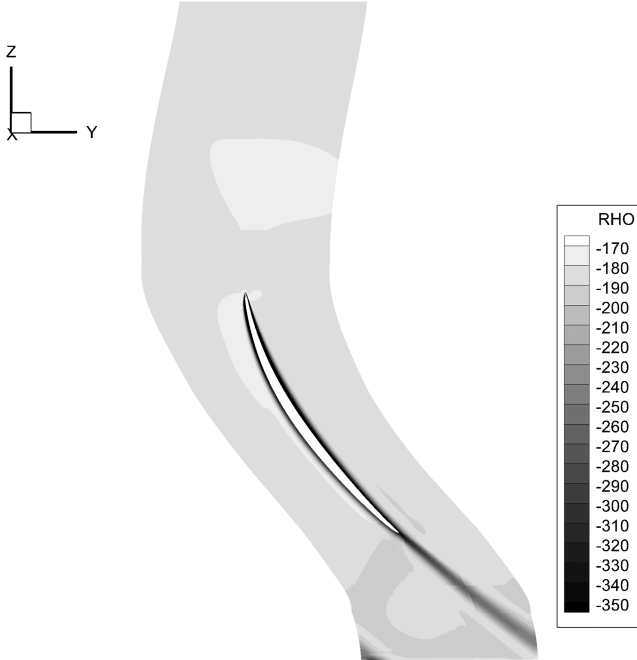


**Fig. 2** Contours of adjoint field for density for efficiency. Nonlinear flow is from bottom to top.

#### IV. Results

This section includes four examples, a commercial engine fan, a compressor rotor, a compressor stator, and a low-pressure turbine cascade. In each of these examples, the different uses of the adjoint solution are highlighted.

Finally, the validity of the “physical insights” into the adjoint solution are established, by using it on a turbine strut. In this case, the goal is to induce end-wall treatments that result in improved performance.

##### A. Commercial Fan

The first example is a commercial fan operating at design conditions. The interest is in the adjoint solutions for the efficiency and the mass flow. The former is a performance measure  $\mathcal{F}$  that one hopes to improve, and the latter is a constraint  $C$  that one wishes to respect during the design optimization. The steady state of the flow was computed using a two-equation model ( $k-\omega$ ), and the adjoint solution was computed using the constant-eddy viscosity approach.

Contours of the density field of the adjoint solution for efficiency and mass flow are shown in Figs. 2 and 3. These contours are roughly at midspan. The adjoint field for efficiency suggests the geometry changes that induce larger reduction in density over the entire pressure surface. This can be achieved through a reduction in camber. On the suction surface, near the front portion of the airfoil, the necessary reduction in density is smaller (than on the pressure surface). Reducing camber to accommodate the design guidance for the pressure surface will only lead to an increase in density over the suction surface (assuming no flow separation due to off-incidence conditions). Hence, to achieve the necessary reduction in density for the leading edge portion of the suction surface, the camber changes have to be offset by thickness increases. Toward the trailing edge, the suction and pressure surface show a desire to reduce the density by equal amounts. These overall changes can be induced by reducing camber for the front portion of the airfoil along with half-thickness increases to provide more curvature to the suction surface, while the portion near the trailing edge requires a combination of camber reduction and reduction in thickness.

The adjoint field for mass flow (drawn with same range as the efficiency plots for clarity) shows a trend similar to the efficiency plot. Hence, if one tries to achieve higher efficiency by lowering the density for the suction surface and the pressure surface, then the mass flow will also increase. If mass flow is a constraint (as is typically the

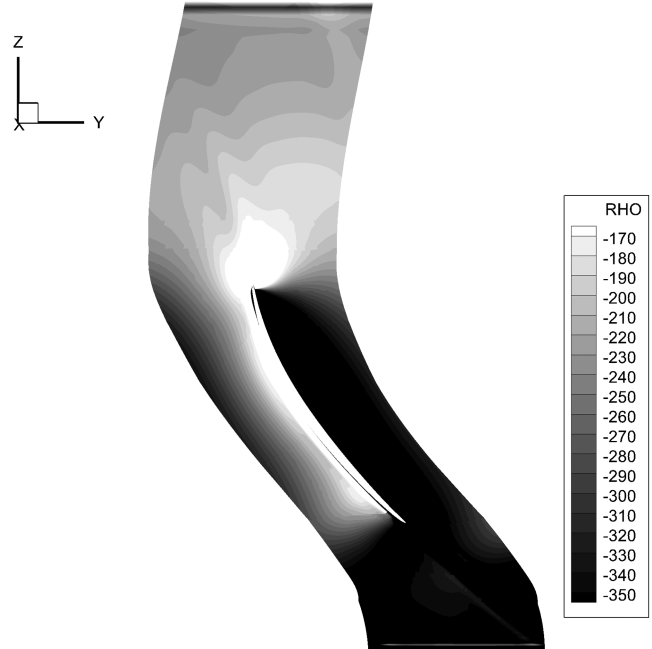


**Fig. 3** Contours of adjoint field for density for mass flow. Nonlinear flow is from bottom to top.

case to ensure fair comparison of the efficiency), then these plots suggest that room for improvement in efficiency for this section of the fan blade may be small.

To evaluate these insights, some design variables are used in an optimization routine. Four design variables are chosen: 1) one that alters the camber distribution in a linear fashion along the leading edge from hub to midspan ( $X_1$ ), 2) one that alters the camber distribution along the leading edge from midspan to tip in a linear fashion ( $X_2$ ), 3) one that alters the camber distribution along the trailing edge from hub to midspan ( $X_3$ ), and 4) one that alters the camber distribution along the trailing edge from midspan to tip ( $X_4$ ). A mesh with about 1 million grid points was used for the simulation and the flow was converged with the  $k-\omega$  turbulence model. The adjoint equations were converged with the constant-eddy viscosity approach.

Figure 4 shows the comparison of the components of the adjoint and finite-difference gradient vector for efficiency, and the comparison is remarkably good. The maximum error is less than 0.2%.

Figure 5 shows the design space around the baseline. The contours were obtained by performing a DOE, while the gradient vector was obtained using the adjoint. White corresponds to regions of higher efficiency, and black corresponds to regions of lower efficiency. The design space shows that the design space between  $X_1$  and  $X_2$ ,

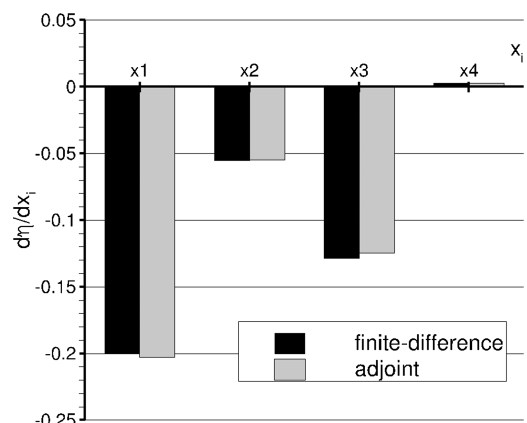


**Fig. 4** Comparison of gradient components for efficiency with finite-difference.

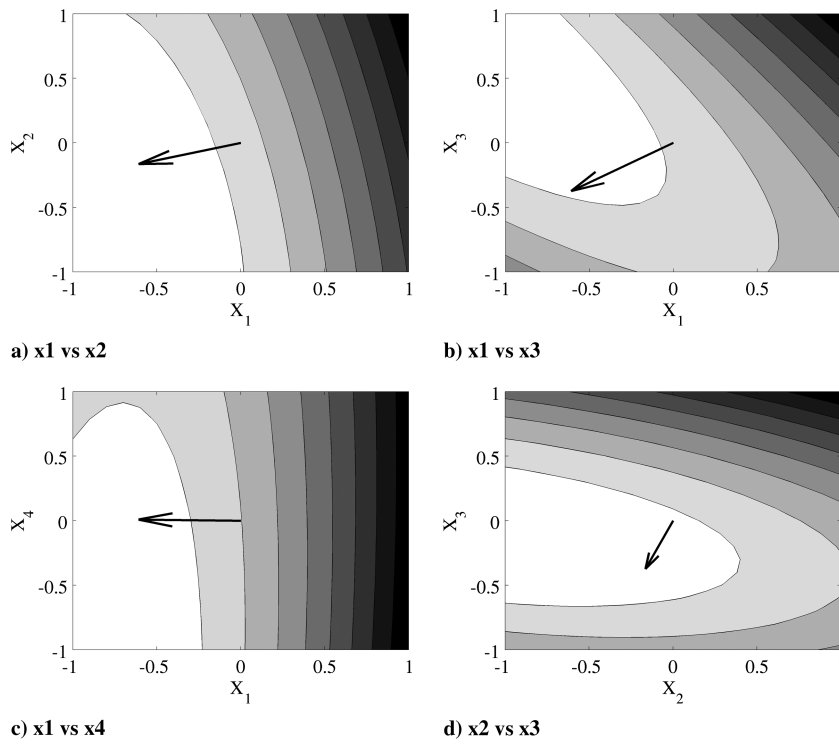


Fig. 5 Directions in design space. The vector is the direction that the adjoint vector points in.

at  $(X_3, X_4) = (0, 0)$ , is roughly quadratic, that between  $X_1$  and  $X_3$ , at  $(X_2, X_4) = (0, 0)$ , shows strong interaction. The small sign inconsistency in the gradient for  $X_4$  is reflected in the nature of the design space being relatively flat.

Finally, Fig. 6 shows the change in efficiency with iterations. Overall, there is about a tenth of a point in improvement in efficiency, suggesting that this blade is already at around the optimum. This improvement in efficiency has been obtained with a 0.13% change in mass flow over the baseline.

#### B. Compressor Rotor

The next example is a compressor rotor blade. Again two metrics are examined, efficiency and pressure ratio and the adjoint field are produced using the constant-eddy viscosity model. In this case, these metrics are considered as objective functions  $\mathcal{F}$ . The pressure ratio is roughly the ratio of the pressure at the exit to the inlet of the domain. Figure 7 shows the adjoint density contours on a cut through the domain for efficiency and pressure ratio.

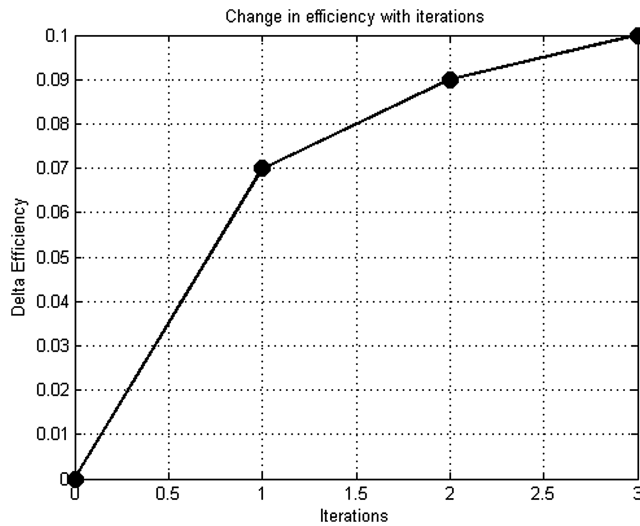


Fig. 6 Change in efficiency with iterations.

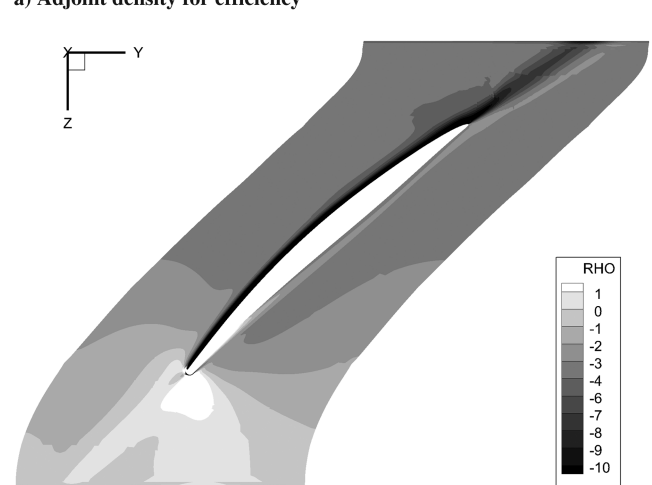
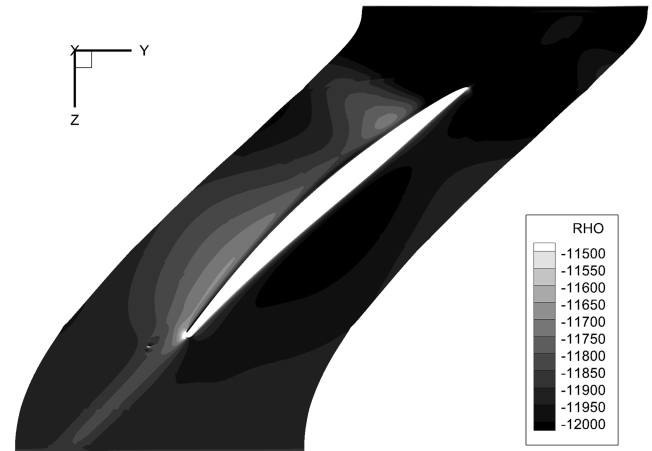


Fig. 7 Adjoint density contours for efficiency and pressure ratio. Nonlinear flow is from bottom to top.

The range in the plot of efficiency is rather narrow and all negative on this plane. This suggests that all portions of the blade are equally sensitive to the metric of interest. On the suction surface, reduction in density is more near the leading-edge region and roughly around midchord, suggesting a geometry change that increases thickness and/or camber. The plot for pressure ratio is shown on a different scale, suggesting that relative to efficiency the changes in density are smaller to affect pressure ratio. The plot also suggests an overall decrease of density over the entire suction surface to cause an increase in pressure ratio. One way to achieve these changes is through a series of localized changes to mean lines.

Figure 8 shows the perturbation produced by a set of bumps on the blade camber-line angle, evenly distributed along the blade chord (30, 50, and 70%) and span (30, 50, and 70%).

An unconstrained maximization optimization problem is run, using the efficiency as the cost function and the previously described nine Hicks–Henne bumps [31] on the camber-line angle used as design variables, as shown in Fig. 8.

The relative evolution of the cost function using a gradient-based optimizer based on the steepest descent method is illustrated in Fig. 9, where the initial efficiency value is used as reference. As it can be

seen, in this unconstrained optimization there was the possibility to improve the efficiency by about 0.16 points but a more realistic exercise would have been to include constraints on the flow. The improvement can be obtained with either the full-adjoint or the CEV model for adjoint.

### C. Compressor Stator

The next example is a compressor stator blade. Here, only one metric is examined, namely the loss. Figure 10 shows contours of the adjoint field for density.

Outside the vicinity of the boundary layer, the contours suggest that on the suction side one should decrease the density flux to decrease loss. The pressure side field suggests a similar change but of smaller magnitude. Along the boundary layer, the adjoint field suggests an increase in density flux for both the pressure and suction side to cause a reduction in loss. This can be achieved by providing more curvature to the suction side and reducing the curvature of the pressure side. Both these changes will provide less blockage to the flow leading to lower losses.

These changes are intuitive for a designer and not of immediate value for this flow. In such cases, the value of the adjoint is in

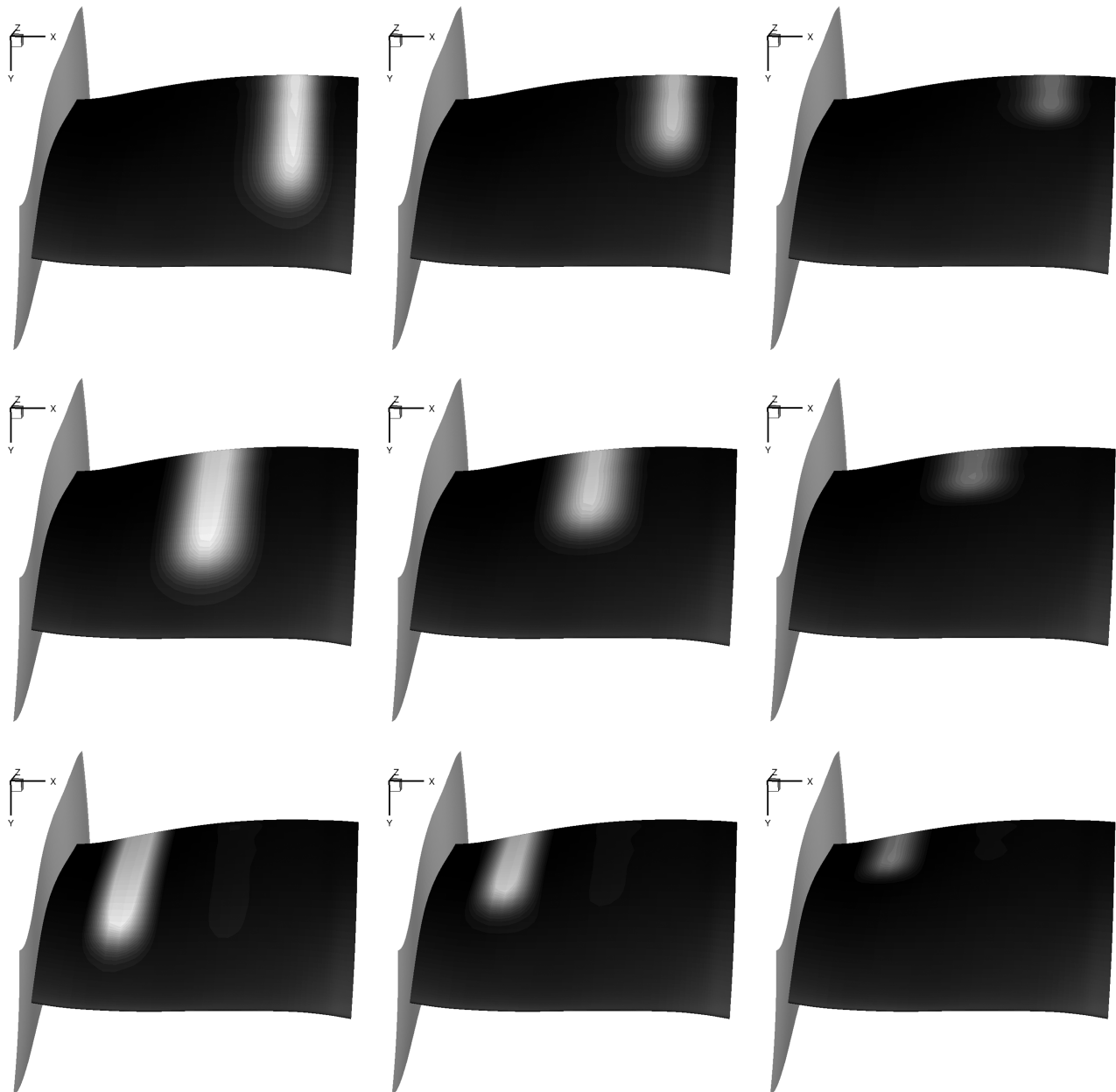


Fig. 8 Hicks–Henne bumps applied to the blade camber-line angle.

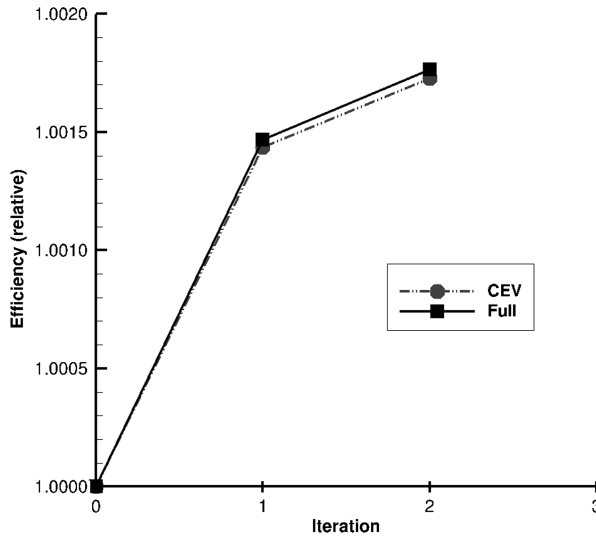
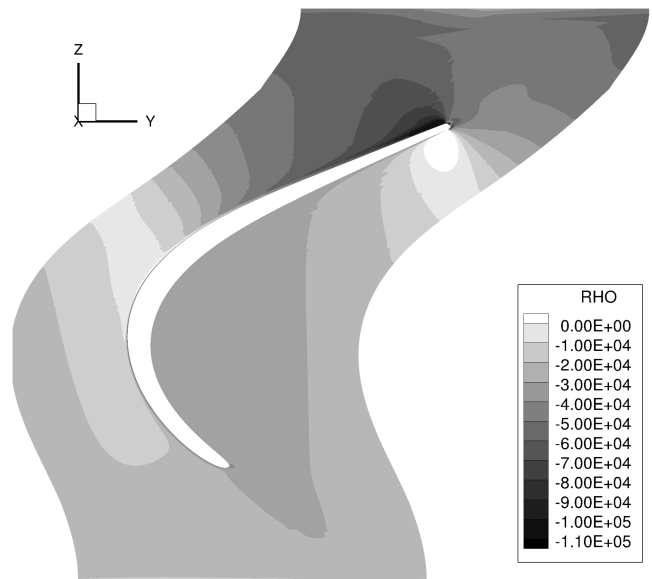


Fig. 9 Optimization test: maximization of efficiency.



a) Adjoint density contours

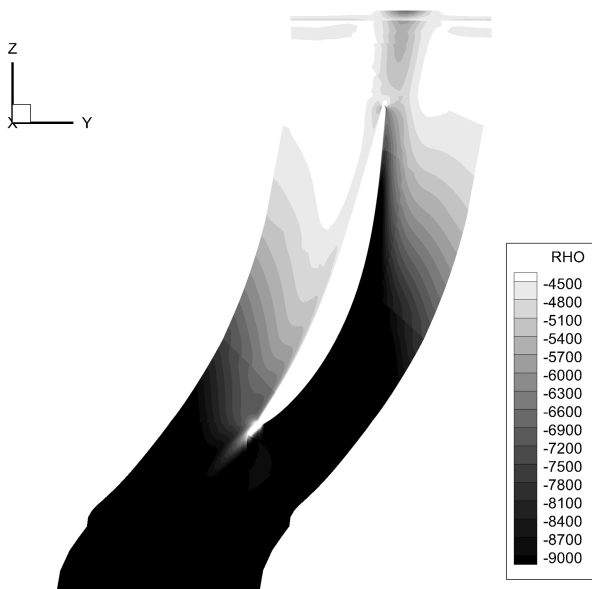
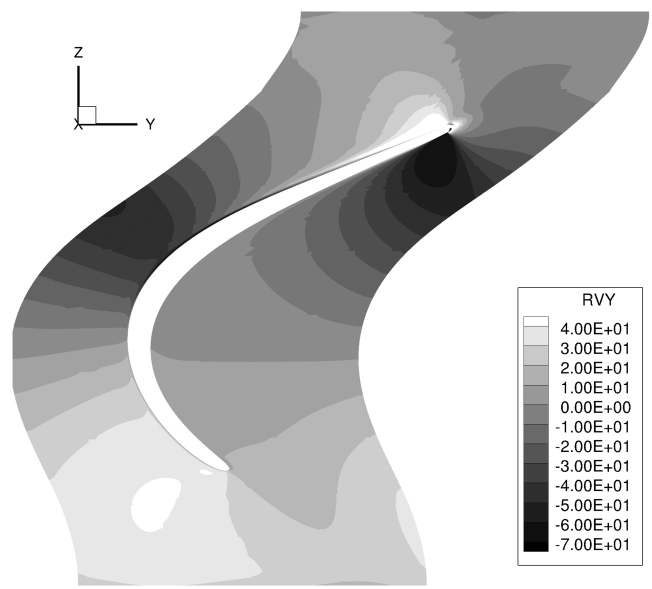


Fig. 10 Contours of adjoint field for density for loss. Nonlinear flow is from bottom to top.



b) Adjoint rho v\_y contours

Fig. 11 Two-dimensional vane adjoint solution for mass flow.

providing quantitative estimates of the geometrical change for use within an optimizer.

#### D. Low-Pressure Turbine Vane

This result has been discussed in Sec. II. Here, the focus is on another metric of interest, namely the mass flow. Figure 11 shows the adjoint density and  $\rho v_y$  contours for mass flow ( $v_y$  is the tangential component of velocity).

These plots show three regions where increases in mass flow can be achieved. The leading edge on the suction side can contribute to increases in mass flow by increasing the camber and/or the thickness. This will accelerate the flow even further, leading to a decrease in the density and an increase in the tangential velocity. The midpassage section on the suction surface can be altered to increase the mass flow by making it thinner. As suggested by the contours, this will cause the local increase in density and the decrease in local tangential velocity. Near the trailing edge, reducing the metal angle (measured from the vertical) will lead to a decrease in tangential velocity on the pressure side and a corresponding increase on the suction side. Overall, these effects can also be simulated by a variety of other geometric changes.

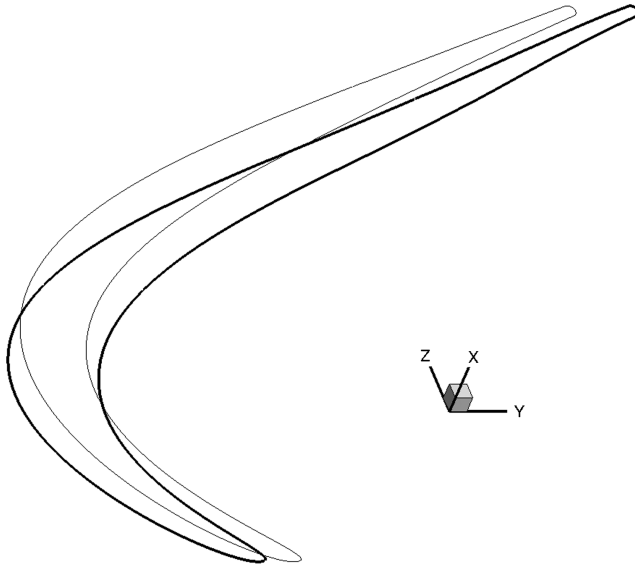
To evaluate this hypothesis, the adjoint solutions are used in an optimization routine with two design variables. The engineering design variables used in this test case are the stagger angle and the overturning angle, as illustrated in Fig. 12.

A sample optimization application, an unconstrained minimization optimization problem using the loss coefficient as the cost function is performed. Two separate runs are performed, one using the full RANS adjoint solver and another the CEV approximation solver.

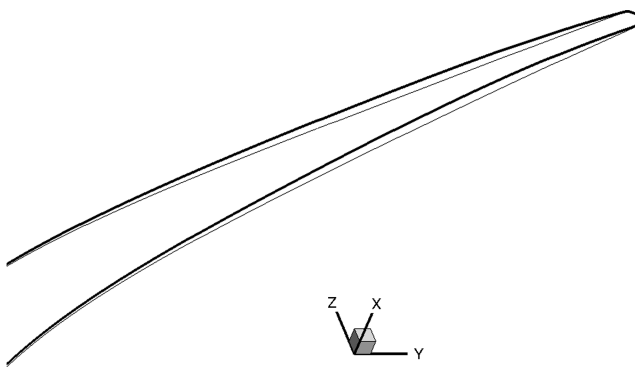
The relative evolution of the cost function using a gradient-based optimizer based on the steepest descent method is illustrated in Fig. 13, where the initial loss coefficient value is used as reference.

#### E. End-Wall Contouring

The adjoint solution is now used to study the effect of end-wall contouring. This is a vane, and hence the loss across the vane is used as the metric to improve. The geometry is skewed (for proprietary reasons), but the plot in Fig. 14 shows the portions of the geometry that the adjoint is suggesting to improve. Loss is most sensitive to the portion of the blade where the adjoint density is dark gray, and an



a) Stagger angle



b) Overturning angle

Fig. 12 Changes applied to the vane geometry.

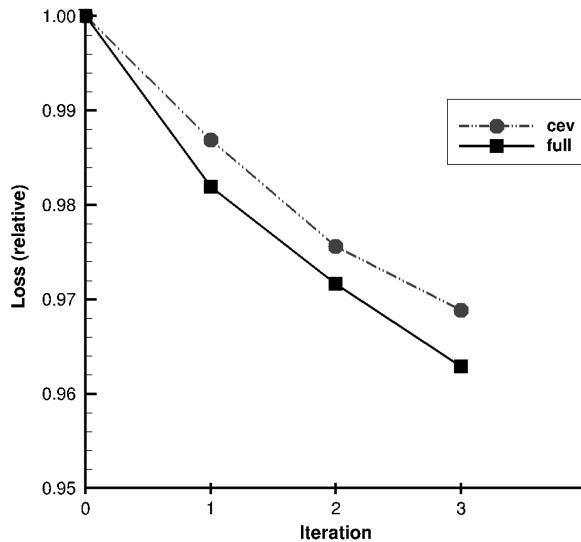


Fig. 13 Two-dimensional vane minimization of loss coefficient.

overall decrease is suggested by the adjoint field. The light gray portions on the casing surface suggest that contouring the end wall to decrease the density there helps improve the loss metric. However, as the goal is to reduce loss, one needs to increase density. This increase can be realized by opening the flow path through end-wall features called troughs [32].

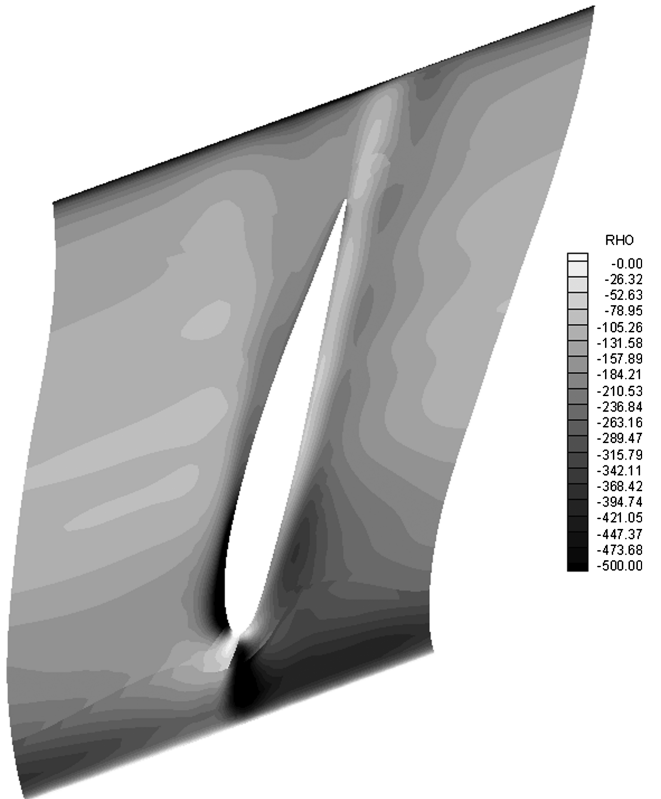


Fig. 14 Contours of adjoint field for density for loss. Nonlinear flow is from bottom to top.

The changes to the end-wall contouring were included in an optimization routine. Typically, without prior knowledge of the important design variables, one chooses a discrete set of shapes that alter the end-wall shape and performs a DOE. The results of this DOE are used to fit a regression or metamodel representation of the design space. The computational cost of this approach scales with the number of design variables. Hence, any method that identifies the important variables helps to reduce the computational cost. It is here that the adjoint solution becomes handy. The adjoint solution and its guidance can be used to determine the most important design variables.

One characterization of the design variables is a parametric  $(u, v)$  representation of the design space; here, Bézier control points positioned in  $(u, v)$  space can be used to alter the shape. It is not uncommon for this parametrization to lead to design variables in the order of a hundred. Typically, these Bézier control points produce troughs and peaks on the casing, and these have been known to reduce cross passage secondary flows, thus leading to reduced loss [32].

With the adjoint guidance, the design variables were reduced to about four: two to control the light gray portion in midpassage (suction and pressure), one around aft pressure side, and one around the leading edge. These correspond to altering the shape in the regions marked in light gray and dark gray in Fig. 14. Near the leading edge, the adjoint solution suggests a rapid variation in density, which will require finer control of the shape changes, which produces valleys and troughs. With this reduced set of design variables, a DOE was performed to determine the optimal shape. Although details of the optimal shape cannot be reported, in an unconstrained design space it was possible to identify shapes that resulted in close to 8% reduction in loss, primarily by altering the midpassage contour, leading-edge, and rear portion of pressure side features. It must be pointed out that these shapes are not realizable due to manufacturing constraints, but nevertheless it shows that the adjoint field can be used for design guidance in new design spaces.

## V. Conclusions

The results from this study show that it is possible to derive physical understanding from the adjoint solution. Each adjoint

variable quantifies the sensitivity of the corresponding conserved flux quantity in the governing Navier–Stokes equations to the metric of interest. Although this is not useful for regular design problems (where the changes to be induced in the geometry are well known and what is usually unknown is the amount of change that needs to be applied), this is invaluable in the following two situations: 1) when there is scant design guidance, and 2) when one needs to gain some understanding into the changes in the flowfield. There are numerous instances of the former and the latter in the turbomachinery design world that will benefit from the study presented in this paper.

The use of adjoint guidance was demonstrated for single-objective optimization problems; however, most relevant industrial problems are multi-objective. Although more research needs to be done to mathematically extend the formulation to multi-objective problems, a possible extension could be along the following lines: from a multiple adjoint solutions for the objectives and constraints, the relative impact of geometry modifications from each adjoint solution can be used to determine if improvements in one objective lead to concurrent improvements in other objectives or not. This implies that all the metrics are scaled so that the different adjoint solutions can be compared or care must be taken in quantitatively measuring the effect of the adjoint solution.

## Appendix: A Sample One-Dimensional Problem

Consider the one-dimensional constant coefficient wave equation. This equation, valid over an  $(t, x)$  domain  $[0, T] \times [0, l]$  along with the initial condition, can be written as

$$\frac{\partial u}{\partial t} + c \frac{\partial u}{\partial x} = 0 \quad u(0, .) = u_0 \quad (\text{A1})$$

and a terminal cost function  $F(T) = \int_0^l |u| dx$ . The adjoint equation for  $u_0 > 0 \quad \forall x$  is

$$-\frac{\partial \psi}{\partial \tau} - c \frac{\partial \psi}{\partial x} = 0 \quad \psi(T, .) = 1 \quad (\text{A2})$$

where  $\tau = -t$ . At terminal time,  $T$ , the adjoint solution over the domain is a constant, and this is the initial condition for the adjoint equation. The adjoint equation is similar to a wave equation with a constant speed of propagation of  $c$ . As the boundary conditions at  $x = 0, l$  do not change, the solution of the adjoint equation is a constant (same as initial condition) over the interval  $[0, T]$ . Hence, the adjoint solution suggests that for any time  $t \in [0, T]$ , the solution  $u$  has to be increased to increase the cost function. This agrees with the form of the cost function. If the initial condition,  $u_0$ , is varied linearly from 1 to  $-1$  over the spatial interval (with a crossover between positive and negative regions happening at  $l/2$ ), then the adjoint solution for the same objective function will be the solution to the backward propagating step-function whose form at time  $T$  has a shock at  $l/2$ . This would suggest that if changes are made to increase  $u$  where the adjoint solution is positive and decrease it where  $u$  is negative, then the objective function will be increased. As the objective function is an absolute function, this interpretation of the adjoint solution is also true.

## Acknowledgments

The authors would like to thank Daniel Wilkin, Dave Cherry, and Lyle Dailey from GE Aviation for their support and feedback. Moreover, the authors are thankful to General Electric for giving permission to publish this paper.

## References

- [1] Nocedal, J., and Wright, S. J., *Numerical Optimization*, Springer, New York, NY, 1999, pp. 421–592.
- [2] Griewank, A., *Evaluating Derivatives*, Society for Industrial and Applied Mathematics, Philadelphia, PA, 2000, pp. 13–118.
- [3] Pironneau, O., “On Optimum Design in Fluid Mechanics,” *Journal of Fluid Mechanics*, Vol. 64, No. 1, 1974, pp. 97–110.  
doi:10.1017/S0022112074002023
- [4] Jameson, A., “Aerodynamic Design via Control Theory,” *Journal of Scientific Computing*, Vol. 3, No. 3, 1988, pp. 233–260.  
doi:10.1007/BF01061285
- [5] Jameson, A., Pierce, N. A., and Martinelli, L., “Optimum Aerodynamic Design Using the Navier–Stokes Equations,” *Theoretical and Computational Fluid Dynamics*, Vol. 10, No. 1–4, 1998, pp. 213–237.  
doi:10.1007/s001620050060
- [6] Reuther, J. J., Alonso, J. J., Jameson, A., Rimlinger, M. J., and Saunders, D., “Constrained Multipoint Aerodynamic Shape Optimization Using an Adjoint Formulation and Parallel Computers, Part 1,” *Journal of Aircraft*, Vol. 36, No. 1, 1999, pp. 51–60.  
doi:10.2514/2.2413
- [7] Martins, J. R. R. A., Alonso, J. J., and Reuther, J. J., “High-Fidelity Aerostructural Design Optimization of a Supersonic Business Jet,” *Journal of Aircraft*, Vol. 41, No. 3, 2004, pp. 523–530.  
doi:10.2514/1.11478
- [8] Marta, A. C., and Alonso, J. J., “Toward Optimally Seeded Airflow on Hypersonic Vehicles Using Control Theory,” *Computers & Fluids*, Vol. 39, No. 9, Oct. 2010, pp. 1562–1574.  
doi:10.1016/j.compfluid.2010.05.009
- [9] Jameson, A., “Aerodynamic Shape Optimization Using the Adjoint Method,” *VKI Lecture Series on Aerodynamic Drag Prediction and Reduction*, von Karman Institute of Fluid Dynamics, Sint-Genesius-Rode, Belgium, Feb. 2003, pp. 3–7.
- [10] Giles, M. B., and Pierce, N. A., “An Introduction to the Adjoint Approach to Design,” *Flow, Turbulence and Combustion*, Vol. 65, Nos. 3–4, 2000, pp. 393–415.  
doi:10.1023/A:1011430410075
- [11] Chung, H.-S., and Alonso, J. J., “Using Gradients to Construct Cokriging Approximation Models for High-Dimensional Design Optimization Problems,” *40th AIAA Aerospace Sciences Meeting and Exhibit*, AIAA Paper 2002-0317, Jan. 2002.
- [12] Laurenceau, J., and Sagaut, P., “Building Efficient Response Surfaces of Aerodynamic Functions with Kriging and Cokriging,” *AIAA Journal*, Vol. 46, No. 2, 2008, pp. 498–507.  
doi:10.2514/1.32308
- [13] Bompard, M., Peter, J., and Desideri, J.-A., “Surrogate Models Based on Function and Derivative Values for Aerodynamic Global Optimization,” *CD-ROM Proceedings of the 5th European Conference on Computational Fluid Dynamics (ECCOMAS CFD 2010)*, edited by Eberhardsteiner, J., Böhm, H. J., and Rammerstorfer, F. G., Instituto Superior Tecnico, Lisbon, Portugal, June 2010.
- [14] Luo, J., Xiong, J., Liu, F., and McBean, I., “Three-Dimensional Aerodynamic Design Optimization of a Turbine Blade by Using an Adjoint Method,” *Journal of Turbomachinery*, Vol. 133, No. 1, 2011, p. 011026.  
doi:10.1115/1.4001166
- [15] He, L., and Wang, D. X., “Concurrent Blade Aerodynamic-Aero-Elastic Design Optimization Using Adjoint Method,” *Journal of Turbomachinery*, Vol. 133, No. 1, 2011, p. 011021.  
doi:10.1115/1.4000544
- [16] Wang, D. X., and He, L., “Adjoint Aerodynamic Design Optimization for Blades in Multistage Turbomachines, Part 1: Methodology and Verification,” *Journal of Turbomachinery*, Vol. 132, No. 2, April 2010, p. 021011.  
doi:10.1115/1.3072498
- [17] Corral, R., and Gisbert, F., “Proled End Wall Design Using an Adjoint Navier–Stokes Solver,” *Journal of Turbomachinery*, Vol. 130, No. 2, 2008, p. 021011.  
doi:10.1115/1.2751143
- [18] Marta, A. C., Mader, C. A., Martins, J. R. R. A., van der Weide, E., and Alonso, J. J., “A Methodology for the Development of Discrete Adjoint Solvers Using Automatic Differentiation Tools,” *International Journal of Computational Fluid Dynamics*, Vol. 21, Nos. 9–10, 2007, pp. 307–327.  
doi:10.1080/10618560701678647
- [19] Mader, C. A., Martins, J. R. R. A., Alonso, J. J., and van der Weide, E., “Adjoint: An Approach for the Rapid Development of Discrete Adjoint Solvers,” *AIAA Journal*, Vol. 46, No. 4, 2008, pp. 863–873.  
doi:10.2514/1.29123
- [20] Wilcox, D. C., “Reassessment of the Scale-Determining Equation for Advanced Turbulence Models,” *AIAA Journal*, Vol. 26, No. 11, Nov. 1988, pp. 1299–1310.  
doi:10.2514/3.10041
- [21] Jameson, A., Schmidt, W., and Turkel, E., “Numerical Solution of the Euler Equations by Finite Volume Methods Using Rung–Kutta Time-Stepping Schemes,” *14th AIAA Fluid and Plasma Dynamic Conference*, AIAA Paper 1981-1259, June 1981.
- [22] Wilcox, D. C., *Turbulence Modeling for CFD*, 2nd ed., DCW Industries, La Cañada, CA, 2002, pp. 83–94.

- [23] Launder, B. E., and Sharma, B. I., "Application of the Energy Dissipation Model of Turbulence to the Calculation of Flow Near a Spinning Disc," *Letters in Heat and Mass Transfer*, Vol. 1, No. 2, 1974, pp. 131–138.  
doi:10.1016/0094-4548(74)90150-7
- [24] Menter, F. R., "Two-Equation Eddy-Viscosity Turbulence Models for Engineering Applications," *AIAA Journal*, Vol. 32, No. 8, 1994, pp. 1598–1605.  
doi:10.2514/3.12149
- [25] Cusdin, P., and Müller, J.-D., "On the Performance of Discrete Adjoint CFD Codes Using Automatic Differentiation," *International Journal of Numerical Methods in Fluids*, Vol. 47, Nos. 8–9, March 2005, pp. 939–945.  
doi:10.1002/fld.885
- [26] Hascoët, L., and Pascual, V., "Extension of TAPENADE Towards Fortran 95," *Automatic Differentiation: Applications, Theory, and Tools*, Lecture Notes in Computational Science and Engineering, edited by Bücker, H. M., Corliss, G., Hovland, P., Naumann, U., and Norris, B., Springer, New York, NY, 2005, pp. 171–179.
- [27] Balay, S., Brown, J., Buschelman, K., Eijkhout, V., Gropp, W. D., Kaushik, D., Knepley, M. G., McInnes, L. C., Smith, B. F., and Zhang, H., "PETSc Users Manual," Argonne National Lab. TR-ANL-95/11, Downers Grove Township, IL, Rev. 3.3, 2012.
- [28] Saad, Y., and Schultz, M. H., "GMRES: A Generalized Minimal Residual Algorithm for Solving Nonsymmetric Linear Systems," *SIAM Journal for Scientific and Statistical Computing*, Vol. 7, No. 3, July 1986, pp. 856–869.  
doi:10.1137/0907058
- [29] Zymaris, A. S., Papadimitriou, D. I., Giannakoglou, K. C., and Othmer, C., "Continuous Adjoint Approach to the Spalart–Allmaras Turbulence Model for Incompressible Flows," *Computers & Fluids*, Vol. 38, No. 8, Sept. 2009, pp. 1528–1538.  
doi:10.1016/j.compfluid.2008.12.006
- [30] Marta, A. C., and Shankaran, S., "On the Handling of Turbulence Equations in RANS Adjoint Solvers," *Computers & Fluids*, Vol. 74, No. 1, 2013, pp. 102–113.  
doi:10.1016/j.compfluid.2013.01.012
- [31] Hicks, R. M., and Henne, P. A., "Wing Design by Numerical Optimization," *Journal of Aircraft*, Vol. 15, No. 7, 1978, pp. 407–412.  
doi:10.2514/3.58379
- [32] Barr, B., Venugopal, P., and Shankaran, S., "Towards Efficient Multidisciplinary Optimization for Turbine Endwall Contouring," *CD-ROM Proceedings of the 6th European Congress on Computational Methods in Applied Sciences and Engineering (ECCOMAS 2012)*, edited by Eberhardsteiner, J., Böhm, H. J., and Rammerstorfer, F. G., Vienna University of Technology, Vienna, Austria, Rept. 3540, Sept. 2012.

J. R. R. A. Martins  
Associate Editor